




# Universal non-Debye low-frequency vibrations in sheared amorphous solids

Vishnu V. Krishnan <sup>\*</sup>, Kabir Ramola <sup>†</sup> and Smarajit Karmakar <sup>‡</sup>

Centre for Interdisciplinary Sciences, Tata Institute of Fundamental Research, Hyderabad 500046, India

(Dated: December 14, 2021)

We study energy minimized configurations of amorphous solids with a simple shear degree of freedom. We show that the low-frequency regime of the vibrational density of states of structural glass formers is crucially sensitive to the stress-ensemble from which the configurations are sampled. In both two and three dimensions, a shear-stabilized ensemble displays a  $D(\omega_{\min}) \sim \omega_{\min}^5$  regime, as opposed to the  $\omega_{\min}^4$  regime observed under unstrained conditions. We also study an ensemble of two dimensional, strained amorphous solids near a plastic event. We show that the minimum eigenvalue distribution at a strain  $\gamma$  near the plastic event occurring at  $\gamma_P$ , displays a collapse when scaled by  $\sqrt{\gamma_P - \gamma}$ , and with the number of particles as  $N^{-0.22}$ . Notably, at low-frequencies, this scaled distribution displays a robust  $D(\omega_{\min}) \sim \omega_{\min}^6$  power-law regime, which survives in the large  $N$  limit. Finally, we probe the universal properties of this ensemble through a characterization of the second and third eigenvalues of the Hessian matrix near a plastic event.

*Introduction:* Amorphous solids are well known to display an anomalous temperature dependence in their heat capacity [1, 2]. This has been suggested to originate due to an excess of modes in their vibrational density of states (VDoS), over and above the Debye modes of crystalline systems, and is known as the Boson peak [3]. This behavior is remarkably robust to the details of the models under consideration, as well as the dimension of the system, and has emerged as a hallmark of amorphous solids. Various theoretical models have been proposed in order to reproduce and characterize this behavior [4–11]. Since a primary quantity of interest in the thermodynamic limit are the mechanical properties of solid glasses, the relevant scales to probe are their properties at low-temperatures, corresponding to low-frequencies in the VDoS. Recently, a new vibrational characteristic of glass formers has been identified: a regime displaying a  $D(\omega) \sim \omega^4$  scaling in the density of states [12–22]. Many theoretical models built around two-level systems, replica symmetry breaking, stress-correlations, random matrices and other hypotheses have been proposed as the origin of this behavior [1, 23–33], however the nature of the modes contributing to the  $\omega^4$  behavior are still a subject of active research. In this context, it is important to characterize new, deviant universal features and their connection to microscopic details.

One of the outstanding problems in the field of glass physics is the development of a statistical, microscopic theory explaining their anomalous thermodynamics. Despite considerable theoretical explorations, the best understanding of the glassy regime of matter emerges from simulations. Preparing an athermal, energy minimized ensemble of structural glass-formers allows us to study an ensemble of *rigid* configurations that are amorphous in nature. Although assumed to be mechanically stable, such configurations have been shown to contain an

additional, strain degree of freedom [34, 35]. An otherwise constrained configuration allows for unbalanced shear stresses that may be specific to the simulation parameters [36]. The choice of appropriate stress ensembles is then an important consideration in the study of amorphous solids [37, 38]. While the effect of modulating internal stresses have been studied [39–41], it is pertinent to reexamine the apparent universality [13, 17–19] under physically relevant, macroscopic shear stress ensembles.

In this Letter, we study realistic ensembles of amorphous solids generated through simple shear, most notably used in cyclic shearing protocols. We use a natural control parameter, namely the shear strain, in order to test the sensitivity of the minimum eigenvalue distributions to changes in ensemble. We show that changes in the macroscopic shear-stress ( $\sigma_{xy}$ ) which leave the internal stress distributions invariant, results in a modification of the amorphous VDoS from  $D(\omega) \sim \omega^4$ . We first consider a shear-stabilized ensemble ( $U = U_{\min}(\gamma)$ ) and show that the low-frequency behavior of the VDoS shifts to a novel power-law close to  $D(\omega_{\min}) \sim \omega_{\min}^5$ . Such a constraint is relevant to the study of stable solids which by definition, resist deformations. Additionally, these results point to a link between the  $\omega^4$  regime in the VDoS and the stress fluctuations sustained by the system. We also uncover a new universal distribution of the minimum eigenvalue under an ensemble of fixed strain-distances to a plastic event. Notably, the distribution collapses under suitable scaling of the strain as well as system size. This distribution additionally displays a low-frequency behavior of  $D(\omega_{\min}) \sim \omega_{\min}^6$ .

*Minimum eigenvalue spectrum:* Vibrational properties of a solid may be discerned from the Hessian of the total potential energy  $U[\{\mathbf{r}^{ij}\}] = \sum_{ij} \psi^{ij}$ , where  $\psi^{ij}$  is the interaction potential between particles  $i$  and  $j$  which we assume to be central. This is conveniently represented by the Hessian matrix

$$\mathcal{H}_{\alpha\beta}^{ij}(\mathbf{r}^{ij}) = \frac{\partial^2 U[\{\mathbf{r}^i\}]}{\partial r_{\alpha}^i \partial r_{\beta}^j}, \quad (1)$$

the indexes of which run over dimensions  $\alpha, \beta \in \{x, y, z\}$

\* vishnuvk@tifrh.res.in

† kramola@tifrh.res.in

‡ smarajit@tifrh.res.in

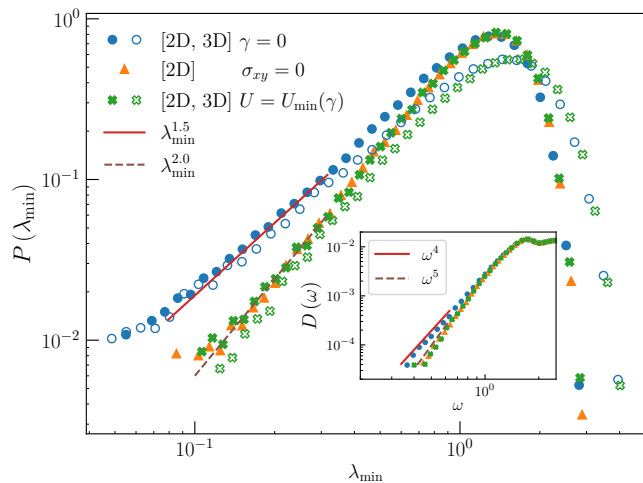


FIG. 1. Minimum eigenvalue distributions obtained from energy minimized configurations of a 2D system of 256 particles. The unfilled markers correspond to a 3D system of 512 particles. The plots compare a typical, *Unstrained* ensemble (blue circles) against the shear-stabilized ensembles: *Zero-shear-stress* (orange triangles) and *Shear-strain-energy-minimized* (green crosses). The distributions drawn from these ensembles deviate significantly from the  $\omega_{\min}^4$  regime. The (red) solid and (violet) dashed lines correspond to power-laws of  $\omega_{\min}^4$  and  $\omega_{\min}^5$  respectively. **(Inset)** Distribution of the *full* vibrational density of states for a 2D system with 256 particles. The low frequency behavior of the distribution is modified from  $D(\omega) \sim \omega^4$  to  $D(\omega) \sim \omega^5$ .

for every pair of particles  $i, j \in \{1, \dots, N\}$ . Above,  $r_{\alpha}^{ij}$  is the  $\alpha$ -component of the distance vector from particle  $i$  to  $j$ . A primary quantity of interest in the study of the vibrational properties of glasses is the distribution of the *minimum* eigenvalue of the Hessian matrix,  $\lambda_{\min}$ . This typically controls the longest time scales in the system, and provides a useful route to characterize the stability of amorphous solids [42].

The vibrational frequencies are related to the eigenvalue of the Hessian as:  $\omega = \sqrt{\lambda}$ . This allows us to relate the two distributions as  $D(\omega) = \sqrt{\lambda}P(\lambda)$ . The distribution of  $\lambda_{\min}$ , being an extreme value distribution is affected by the correlations between the eigenvalues of the Hessian matrix. However, many glass formers display a  $P(\lambda_{\min}) \sim \lambda_{\min}^{1.5} \equiv D(\omega_{\min}) \sim \omega_{\min}^4$  behavior in the tail of the minimum eigenvalue distribution, indicating weak correlations in the low lying eigenvalues [12]. Deviations from this universal behavior are therefore of interest in determining different structural properties of glasses. Indeed, we show in this Letter that the response of short ranged glass formers to shear is linked to changes in  $P(\lambda_{\min})$ , which in turn is crucially sensitive to the stress-ensemble from which configurations are drawn.

*Shear-stabilized ensembles:* We consider configurations that are allowed to undergo volume-preserving, simple shear, where only the upper-triangular elements of the strain tensor can be non-zero ( $\gamma_{\alpha\beta} = \epsilon_{\alpha\beta}^{<\beta}$ ). An

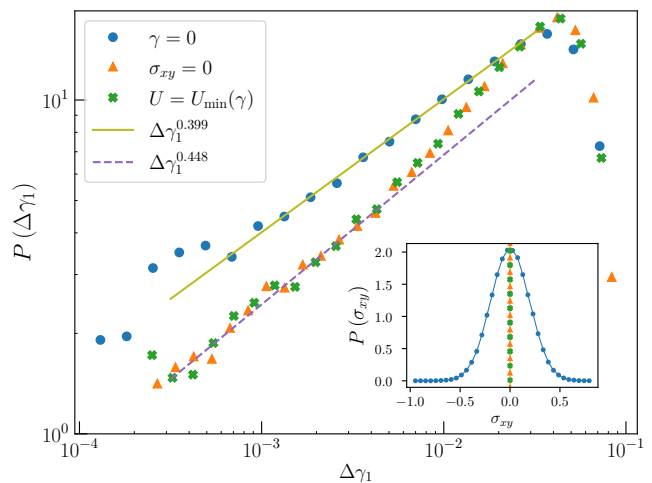


FIG. 2. Distributions of the strain  $\Delta\gamma_1$  required to achieve the first plastic event, beginning with configurations sampled from the unstrained, and from the two shear-stabilized ensembles. These measurements were performed on 2D systems of size  $N = 256$  in two dimensions. The lines indicate best-fits for the exponent. The shear-stabilized ensembles have fewer plastic events at smaller strains. **(Inset)** Distribution of the macroscopic shear stress in energy minimized configurations. The *Unstrained* ensemble displays finite shear-stress fluctuations, while the shear-stabilized ensembles contain configurations with no macroscopic shear stress.

isolated stable solid relaxes along all available degrees of freedom. In such energy minimized configurations of systems comprised of particles interacting via pairwise, central potentials, the off-diagonal element of the macroscopic force moment tensor, i.e., shear stress is exactly zero [43] (see Supplemental Material [44]/1):

$$\frac{\partial U}{\partial \gamma_{\alpha\beta}} = \sum_{\langle i,j \rangle} f_{\alpha}^{ij} r_{\beta}^{ij} = \sum_{\langle i,j \rangle} \sigma_{\alpha\beta}^{ij} \equiv \sigma_{\alpha\beta} \times V, \quad (2)$$

where  $f_{\alpha}^{ij}$  is the  $\alpha$ -component of the force on particle  $i$  by particle  $j$ ,  $\sigma_{\alpha\beta}^{ij}$  is the bond-stress between particles  $i$  and  $j$ ,  $\sigma_{\alpha\beta}$  is the macroscopic stress tensor and  $V$  is the volume of the system. It is therefore natural to probe the effect of macroscopic shear stress fluctuations on the stability properties of such systems, which are enhanced due to relaxation along an additional strain degree of freedom.

In this context, we analyze the distribution of minimum eigenvalues of the Hessian matrices of configurations sampled from two different ensembles with (i) finite shear stress fluctuations and (ii) zero shear stress fluctuations (within a tolerance). The finite stress ensemble appears naturally when generating energy minimized configurations from a thermal ensemble, under periodic boundary conditions (see Supplemental Material [44]/2), and we refer to this as the *Unstrained* ensemble. We create shear-stabilized ensembles using two different procedures. In the first method, we athermally

strain the system in the direction of the shear stress until the stress changes sign, and this is repeated two more times, with reduced strain increments. We term this ensemble *Zero-shear-stress* (Supplemental Material [44]/3 shows the strains required). Such a procedure allows us to attain stress-free states in systems with one shear-stress, namely, systems in two dimensions. Therefore, we also use a technique capable of relaxing stresses in three dimensional systems. In the second method, we perform an energy minimization of the position as well as shear strain degrees of freedom concomitantly, and refer to this ensemble as *Shear-strain-energy-minimized*. Further details of both procedures are described in the Supplemental Material [44]/7. Notably, these protocols leave the statistics of the internal bond-stresses invariant (see Supplemental Material [44]/4).

We display numerically sampled minimum eigenvalue distributions of the Hessian for two (2D) and three dimensional (3D) systems in Fig. 1. Remarkably, the minimum eigenvalue distributions corresponding to the two types of ensembles yield markedly different results, especially at the lowest frequencies which govern large-scale stability properties. Specifically, we find that the well-known  $\omega_{\min}^4$  regime is modified in the shear-stabilized ensembles, and instead we find the best-fit power-law to be closer to  $\omega_{\min}^5$ . For data on larger system sizes, see Supplemental Material [44]/5. Moreover, we find that the two different procedures of generating a shear-stabilized ensemble yield identical distributions, pointing to the fact that these distributions are sensitive to the stress ensemble and not the preparation protocol, independent of dimension.

*Mechanical properties:* Understanding the relationship between microscopic parameters and bulk rigidity is important in constructing a first-principles theory of solids. In order to further probe the connection between the minimum eigenvalue distributions and the stability of configurations created in different stress ensembles, we carry out Athermal Quasistatic Shearing (AQS) of the system [45], using 2D glass structures (see Supplemental Material [44]/7 for details). AQS allows us to trace the state of a local minimum as the potential energy surface is transformed under an effectively infinitesimal strain rate. Amorphous materials as well as crystals, when subjected to an incremental strain, produce a corresponding linear stress-response. However, unlike crystals, amorphous arrangements of particles incur localized, non-affine, displacements termed ‘plastic events’. These deformations are easily identified in an athermal straining protocol by the occurrence of abrupt stress-drops and localized particle displacements. The amorphous nature of the constituent particles allows the system to release stresses via such events that comprise displacements of a small fraction of the particles that occurs when energy minimizing the system after imparting it an affine strain.

The distribution of the strain needed to induce the first plastic event forms an important descriptor of the rigidity of solids, and is an indicator of their stability to shear.

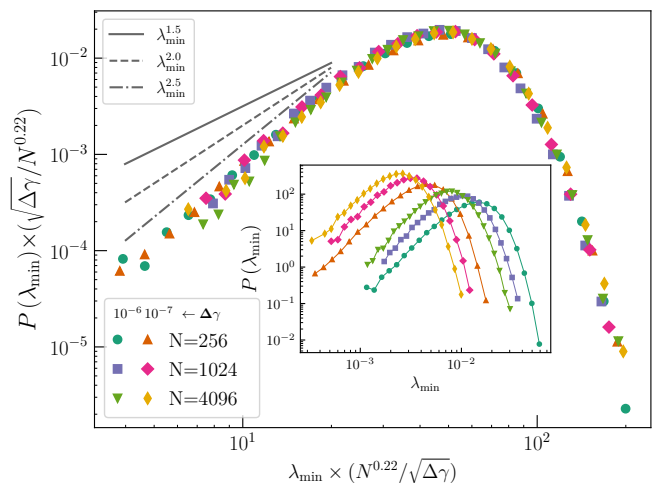


FIG. 3. Distributions of the minimum eigenvalue of the Hessian matrix,  $\lambda_{\min}$ , drawn from strained configurations grouped by distance  $\Delta\gamma$  from their respective first plastic events (**Inset**). These distributions collapse when scaled by the strain gap as  $\sqrt{\Delta\gamma}$  and the number of particles as  $N^{-0.22}$ . These scaled distributions show a marked deviation from  $\omega_{\min}^4$  behavior (solid line). The dash-dotted line corresponds to a power-law of  $\omega_{\min}^6$ .

It is therefore important to study the nature of such distributions in appropriate, experimentally relevant stress-ensembles. As discussed in Eq. (2), the shear-stabilized ensembles with zero shear stress may provide an accurate characterization of the stability of real solids. In Fig. 2 we show that the distribution of the strain  $\Delta\gamma_1$  needed to achieve the first plastic event, is sensitive to the stress-fluctuations allowed in the configurations sampled. Most significantly, the *Unstrained* ensemble is more susceptible to plastic events at lower strain-deformations. Intriguingly, the estimated exponent ( $P(\Delta\gamma_1) \sim \Delta\gamma_1^\theta$ ) in the low  $\Delta\gamma_1$  regime, an important characterization of amorphous stability [46, 47], seems to increase from  $\theta \approx 0.4$  to  $\theta \approx 0.45$  between the unstrained and shear-stabilized ensembles.

*Plastic-event approach ensemble:* Since a primary utility of a Hessian analysis is the determination of the stability of amorphous systems, it is natural to focus on the nature of the ensemble of near-failure amorphous solids. These plastic events correspond to the system crossing saddles in the energy landscape as it is sheared [48]. Traversing across such energy barriers by straining the system allows us to probe the energy landscape that determines the stability of such amorphous configurations of particles. The model system used allows us to study its properties close to such a phenomenon. Once the plastic event is identified, as described in the previous section, we then proceed to ascertain the strain  $\gamma_P$ , at which the plastic event occurs, to a high degree of precision by using very fine strain-steps. This permits us to sample configurations that are arbitrarily close to the

event. We thus define the *Plastic-event-approach* ensemble as a collection of configurations all at the same strain to the plastic event ( $\Delta\gamma = \gamma_P - \gamma$ ).

We study the single most important marker of stability, namely the minimum eigenvalue of the Hessian, as the system approaches the plastic-strain ( $\gamma_P$ ) at which a saddle in the energy landscape is reached. The behavior of the displacement field has been shown to be proportional to the minimum eigenmode, when close to such a plastic event [49]:

$$\mathbf{u}(\gamma) - \mathbf{u}(\gamma_P) = X(\gamma)\Psi_{\min}, \quad (3)$$

where  $\mathbf{u}$  represents the position of the particles as a function of the strain  $\gamma$ , and  $X$  is the projection of the displacement field on to the minimum eigenvector  $\Psi_{\min}$ . The minimum eigenvalue is assumed to vary linearly with the projection  $\lambda_{\min} \approx \alpha X(\gamma)$ , which in-turn leads to an approach to zero with a square-root singularity:  $\lambda_{\min} \approx \alpha\sqrt{\gamma_P - \gamma}$ . This singular behavior occurs due to the eigenvector corresponding to the minimum eigenvalue aligning itself with the displacement vector corresponding to the plastic event. A natural question then is the exact nature of the proportionality constant  $\alpha$  that governs the magnitude of the change in the minimum eigenvalue of the Hessian with the strain of the system. The singular square-root approach is quite general and is expected whenever a system approaches a saddle corresponding to a plastic event along one of its degrees of freedom. For example, a crystalline system undergoing a slip will have its eigenvalue vanish with a single  $\alpha$  determined by the interactions between the particles. On the other hand, amorphous materials differ in that the constant of proportionality  $\alpha$  varies from sample to sample. The statistics of  $\alpha$  is consequently dependent purely on the microscopic parameters of the system, and we therefore expect a universal distribution of the form

$$P(\alpha) \equiv P\left(\frac{\lambda_{\min}}{\sqrt{\gamma_P - \gamma}}\right). \quad (4)$$

In Fig. 3, we display these distributions at small distances to the plastic strain as well as for various system sizes. We scale these distributions with the strain-distance as  $\sqrt{\Delta\gamma}$  and system size as approximately  $N^{-0.22}$ . This universal distribution seems to exhibit a low-frequency power-law of  $\lambda_{\min}^{2.5}$  corresponding to  $\omega_{\min}^6$ . The full approach to the plastic event is illustrated in the Supplemental Material [44]/6. Attempts at fitting one of the three common extreme value distributions failed to yield a reasonable match, suggesting a non-trivial limiting form. Using the estimated exponent  $\alpha \approx 2.5$  in an extreme value fit of uncorrelated variables predicts a scaling with  $N$  with an exponent  $1/(1 + \alpha) \approx 0.286$ . The significant difference from our observed system size scaling exponent of 0.22 also points to correlations in the underlying eigenvalues, which would be interesting to characterize further.

*Second and third eigenvalue distributions:* The Hessian matrices of amorphous systems have also been

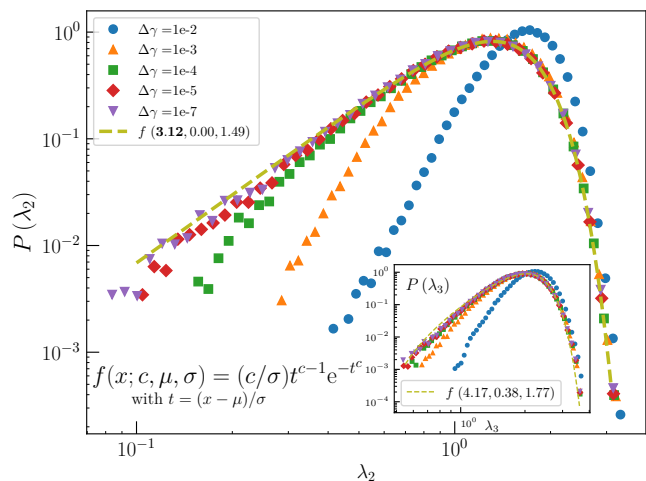



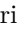

FIG. 4. Distributions of the second eigenvalue of  $N = 256$  systems, as it approaches the plastic event. Surprisingly, the distribution approaches a Weibull form as the plastic event is approached. The dashed line is a two-parameter Weibull fit with  $\mu$  set to 0. **(Inset)** Distribution of the third eigenvalue in the same system. This distribution does not fit well to a generalized extreme value form. The best fit is displayed by the dashed line.

sought to be modeled within Random Matrix frameworks [26, 50–54]. In this context, we analyze the behavior of the second and third eigenvalues  $\lambda_2, \lambda_3$ , as the system approaches a plastic event. Notably, in the limit of a vanishing minimum eigenvalue, the second eigenvalue is equivalent to the first level-spacing. Such near-extreme value distributions are natural measures that arise in Random Matrix Theory [55, 56], and could therefore serve as useful tools to understand the nature of the *ensemble* that the Hessian matrices of amorphous solids generate.

As the plastic event is approached, the minimum eigenvalue departs from the remaining vibrational frequencies. The effect of such a separation is clearly felt by the remnant of the spectrum, as can be seen in Fig. 4. Interestingly, as the system approaches this saddle point, the distribution of the second eigenvalue converges to a zero-located Weibull distribution. Such Weibull forms have also been observed in the minimum eigenvalue distributions in glass formers, for small system sizes [12]. Our best fit curve is displayed in Fig. 4, showing a very good match. Additionally, the fit estimates a low-frequency power-law of about  $\lambda_2^{2.12}$ . Such a characterization assumes relevance when studying solids close to plastic events, because the VDoS may then be well represented by a spectrum with one less mode than otherwise. Finally we also measure the statistics of the third eigenvalue as the plastic event is approached. We plot this distribution in the inset of Fig. 4. Once again, this distribution attains a limiting form. However, this distribution does not seem to fit well with the generalized extreme value distributions.

*Discussion:* We have presented results highlighting the role played by the choice of ensemble in the low-frequency regime of the VDoS of structural glass formers. We find that crucially, finite shear stress fluctuations are required to observe the universal  $\omega_{\min}^4$  regime that has emerged as a hallmark of low-temperature glasses. Determining the appropriate distributions of stresses in real amorphous solids prepared under different conditions, and their effect on structural properties would therefore be of immediate relevance. We also showed that the minimum eigenvalue of the Hessian attains a universal distribution when approaching a plastic event. It would be interesting to probe the origin of the anomalous scaling of  $N^{-0.22}$  with the number of particles displayed by this distribution. The robustness of the  $\omega_{\min}^4$  regime in the VDoS of amorphous solids in the context of our study motivates an analysis of different models of structural glass formers in stress-controlled ensembles, in two as

well as three dimensions. Similarly, studying the effects of varying the smoothness in the interaction potentials which have been shown to have non-trivial effects on the Hessian matrices [57], could help better understand the stability of amorphous solids to shear. Finally, it would also be interesting to study the shear stress fluctuations in ultrastable glasses, which have been shown to have anomalous rigidity properties [58].

*Acknowledgments:* We thank Edan Lerner , Jishnu Nampoothiri  and Srikanth Sastry  for useful discussions. V.V.K. thanks the Council of Scientific and Industrial Research, India for support via the Shyama Prasad Mukherjee Fellowship (SPM-07/1142(0228)/2015-EMR-1). S.K. would like to acknowledge the support from Swarna Jayanti Fellowship Grants No. DST/SJF/PSA-01/2018-19 and No. SB/SFJ/2019-20/05. This project was funded by intramural funds at TIFR Hyderabad from the Department of Atomic Energy, Government of India.

- 
- [1] U. Buchenau, Y. M. Galperin, V. L. Gurevich, and H. R. Schober, *Phys. Rev. B* **43**, 5039 (1991).
- [2] M. A. Ramos, *Philosophical Magazine* **84**, 1313 (2004).
- [3] U. Buchenau, N. Nücker, and A. J. Dianoux, *Phys. Rev. Lett.* **53**, 2316 (1984).
- [4] P. W. Anderson, B. I. Halperin, and C. M. Varma, *Philos. Mag.* **25**, 1 (1972).
- [5] W. A. Phillips, *J. Low Temp. Phys.* **7**, 351 (1972).
- [6] U. Buchenau, A. Wischnewski, M. Ohl, and E. Fabiani, *J. Phys.: Condensed Matter* **19**, 205106 (2007).
- [7] M. Baggioli and A. Zaccane, *Phys. Rev. Lett.* **122**, 145501 (2019).
- [8] A. Zaccane, *J. Phys.: Condensed Matter* **32**, 203001 (2020).
- [9] M. Baggioli and A. Zaccane, *Phys. Rev. Research* **2**, 013267 (2020).
- [10] L. Casella, M. Baggioli, T. Mori, and A. Zaccane, *J. Chem. Phys.* **154**, 014501 (2021).
- [11] M. Baggioli and A. Zaccane, *Int. J. Mod. Phys. B* **35**, 2130002 (2021).
- [12] E. Lerner, G. Düring, and E. Bouchbinder, *Phys. Rev. Lett.* **117**, 035501 (2016).
- [13] G. Kapteijns, E. Bouchbinder, and E. Lerner, *Phys. Rev. Lett.* **121**, 055501 (2018).
- [14] M. Paoluzzi, L. Angelani, G. Parisi, and G. Ruocco, *Phys. Rev. Lett.* **123**, 155502 (2019).
- [15] L. Wang, A. Ninarello, P. Guan, L. Berthier, G. Szamel, and E. Flenner, *Nat. Commun.* **10**, 1 (2019).
- [16] F. Arceri and E. I. Corwin, *Phys. Rev. Lett.* **124**, 238002 (2020).
- [17] D. Richard, K. González-López, G. Kapteijns, R. Pater, T. Vaknin, E. Bouchbinder, and E. Lerner, *Phys. Rev. Lett.* **125**, 085502 (2020).
- [18] S. Bonfanti, R. Guerra, C. Mondal, I. Procaccia, and S. Zapperi, *Phys. Rev. Lett.* **125**, 085501 (2020).
- [19] M. Shimada, H. Mizuno, L. Berthier, and A. Ikeda, *Phys. Rev. E* **101**, 052906 (2020).
- [20] P. Das, H. G. E. Hentschel, E. Lerner, and I. Procaccia, *Phys. Rev. B* **102**, 014202 (2020).
- [21] M. Paoluzzi, L. Angelani, G. Parisi, and G. Ruocco, *Phys. Rev. Research* **2**, 043248 (2020).
- [22] P. Das and I. Procaccia, *Phys. Rev. Lett.* **126**, 085502 (2021).
- [23] V. L. Gurevich, D. A. Parshin, and H. R. Schober, *Phys. Rev. B* **67**, 094203 (2003).
- [24] V. Gurarie and J. T. Chalker, *Phys. Rev. B* **68**, 134207 (2003).
- [25] D. A. Parshin, H. R. Schober, and V. L. Gurevich, *Phys. Rev. B* **76**, 064206 (2007).
- [26] E. Stanifer, P. K. Morse, A. A. Middleton, and M. L. Manning, *Phys. Rev. E* **98**, 042908 (2018).
- [27] H. Ikeda, *Phys. Rev. E* **99**, 050901(R) (2019).
- [28] B. Cui and A. Zaccane, *Eur. Phys. J. E* **43**, 1 (2020).
- [29] E. Bouchbinder, E. Lerner, C. Rainone, P. Urbani, and F. Zamponi, *Low-frequency vibrational spectrum of mean-field disordered systems* (2021).
- [30] M. Shimada, H. Mizuno, and A. Ikeda, *Soft Matter* **17**, 346 (2021).
- [31] M. Shimada, H. Mizuno, and A. Ikeda, *Soft Matter* **16**, 7279 (2020).
- [32] D. A. Conyuh and Y. M. Beltukov, *Phys. Rev. B* **103**, 104204 (2021).
- [33] C. Rainone, P. Urbani, F. Zamponi, E. Lerner, , and E. Bouchbinder, *SciPost Phys. Core* **4**, 8 (2021).
- [34] S. Dagois-Bohy, B. P. Tighe, J. Simon, S. Henkes, and M. van Hecke, *Phys. Rev. Lett.* **109**, 095703 (2012).
- [35] Y. Wu, P. Olsson, and S. Teitel, *Phys. Rev. E* **92**, 052206 (2015); Y. Wu and S. Teitel, *Phys. Rev. E* **91**, 022207 (2015); *Phys. Rev. E* **92**, 022207 (2015).
- [36] Periodic boundary conditions together with the preparation protocols generate configurations corresponding to a non-zero shear stress ensemble due to constrained rotational freedom.
- [37] S. Henkes and B. Chakraborty, *Phys. Rev. E* **79**, 061301 (2009).
- [38] D. Bi, J. Zhang, R. Behringer, and B. Chakraborty, *Europhys. Lett.* **102**, 34002 (2013).
- [39] H. Mizuno, H. Shiba, and A. Ikeda, *Proc. Nat. Acad. Sci.* **114**, E9767 (2017).
- [40] E. Lerner and E. Bouchbinder, *Phys. Rev. E* **97**, 032140

- (2018).
- [41] A. Moriel, *Phys. Rev. Lett.* **126**, 088004 (2021).
  - [42] C. Maloney and A. Lemaître, *Phys. Rev. Lett.* **93**, 195501 (2004).
  - [43] S. Karmakar, E. Lerner, and I. Procaccia, Athermal non-linear elastic constants of amorphous solids (2010), Appendix C, [arXiv:1004.2198 \[cond-mat.stat-mech\]](https://arxiv.org/abs/1004.2198).
  - [44] See Supplemental Material for details, which includes Refs. [59-69].
  - [45] S. Kobayashi, K. Maeda, and S. Takeuchi, *Acta Metallurgica* **28**, 1641 (1980).
  - [46] J. Lin, A. Saade, E. Lerner, A. Rosso, and M. Wyart, *EPL (Europhysics Letters)* **105**, 26003 (2014).
  - [47] J. Lin, E. Lerner, A. Rosso, and M. Wyart, *Proc. Nat. Acad. Sci.* **111**, 14382 (2014).
  - [48] C. E. Maloney and A. Lemaître, *Phys. Rev. E* **74**, 016118 (2006).
  - [49] S. Karmakar, A. Lemaître, E. Lerner, and I. Procaccia, *Phys. Rev. Lett.* **104**, 215502 (2010).
  - [50] Y. M. Beltukov and D. A. Parshin, *Phys. Solid State* **53**, 151 (2011).
  - [51] Y. M. Beltukov, V. I. Kozub, and D. A. Parshin, *Phys. Rev. B* **87**, 134203 (2013).
  - [52] M. L. Manning and A. J. Liu, *Europhys. Lett.* **109**, 36002 (2015).
  - [53] D. A. Conyuh, Y. M. Beltukov, and D. A. Parshin, *J. Phys.: Conf. Ser.* **929**, 012031 (2017).
  - [54] M. Baggioli, R. Milkus, and A. Zaccane, *Phys. Rev. E* **100**, 062131 (2019).
  - [55] M. L. Mehta, *Random Matrices and the Statistical Theory of Energy Levels* (Elsevier, New York, 2014).
  - [56] C. E. Porter, *Statistical Theories of Spectra : Fluctuations* (Academic Press, 1965).
  - [57] V. V. Krishnan, S. Karmakar, and K. Ramola, *Phys. Rev. Research* **2**, 042025(R) (2020).
  - [58] M. Ozawa, L. Berthier, G. Biroli, A. Rosso, and G. Tarjus, *Proc. Nat. Acad. Sci.* **115**, 6656 (2018).
  - [59] S. Plimpton, *J. Comput. Phys.* **117**, 1 (1995).
  - [60] *Large-scale Atomic/Molecular Massively Parallel Simulator*, Sandia National Laboratories (2003), Versions: 5Jun2019,3March2020.
  - [61] E. Anderson, Z. Bai, C. Bischof, S. Blackford, J. Demmel, J. Dongarra, J. Du Croz, A. Greenbaum, S. Hammarling, A. McKenney, and D. Sorensen, *LAPACK Users' Guide*, 3rd ed. (Society for Industrial and Applied Mathematics, Philadelphia, PA, 1999).
  - [62] Intel, *Math Kernel Library* (2019).
  - [63] S. van der Walt, S. C. Colbert, and G. Varoquaux, *Comput. Sci. Eng.* **13**, 22 (2011).
  - [64] C. R. Harris, K. J. Millman, S. J. van der Walt, R. Gommers, P. Virtanen, D. Cournapeau, E. Wieser, J. Taylor, S. Berg, N. J. Smith, *et al.*, *Nature* **585**, 357 (2020).
  - [65] *NumPy, Version: 1.20.1* (2021).
  - [66] P. Virtanen, R. Gommers, T. E. Oliphant, *et al.*, *Nat. Methods* **17**, 261 (2020).
  - [67] *SciPy, Version: 1.6.2* (2021).
  - [68] J. D. Hunter, *Comput. Sci. Eng.* **9**, 90 (2007).
  - [69] *Matplotlib, Version: 3.4.1* (2021).

# Supplemental Material for “Universal non-Debye low-frequency vibrations in sheared amorphous solids”

## 1. Shear-stabilization

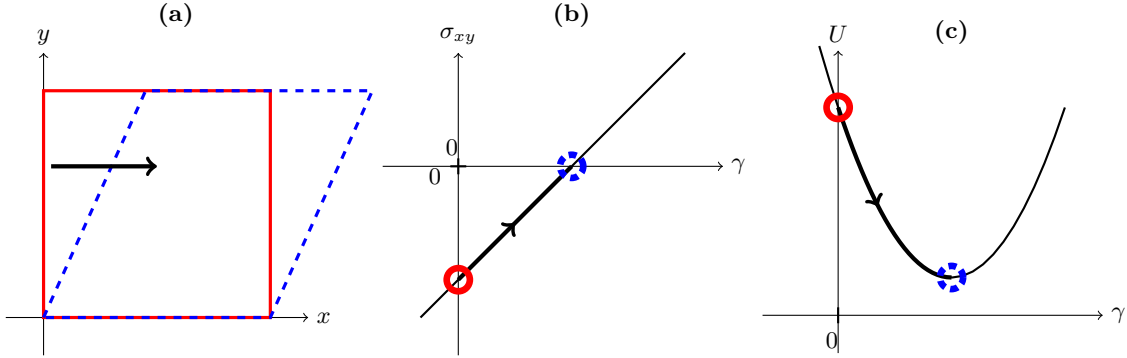


FIG. S1. (a) Schematic representations of a system undergoing simple shear, and corresponding changes in (b) stress and (c) energy. The (red) solid state represents an unstrained state that exhibits a finite shear-stress. The (blue) dashed state represents a shear-stabilized state.

## 2. Stress Fluctuations

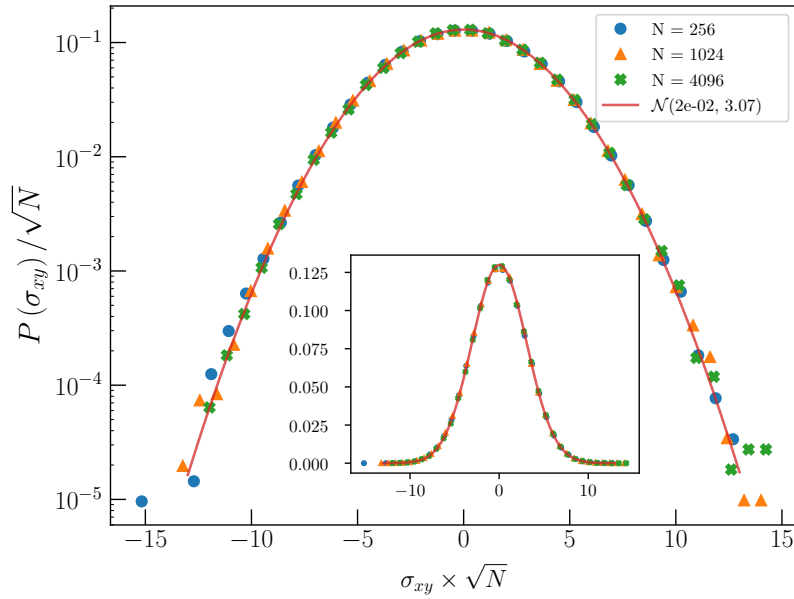


FIG. S2. Stress distributions of configurations generated by cooling and energy-minimizing a thermal ensemble under periodic boundaries. The plot shows the stress fluctuations of system sizes  $N \in \{256, 1024, 4096\}$ . The distributions scale with system size as  $1/\sqrt{N}$  in two dimensions. The solid line is a maximum-likelihood-estimate fit of the Normal distribution to the data corresponding to  $N = 4096$ , with fit parameters shown in the legend. These plots quantify the effective residual stresses present in simulated models of amorphous solids when prepared under unstrained conditions.

### 3. Strain required to achieve Shear-stabilization

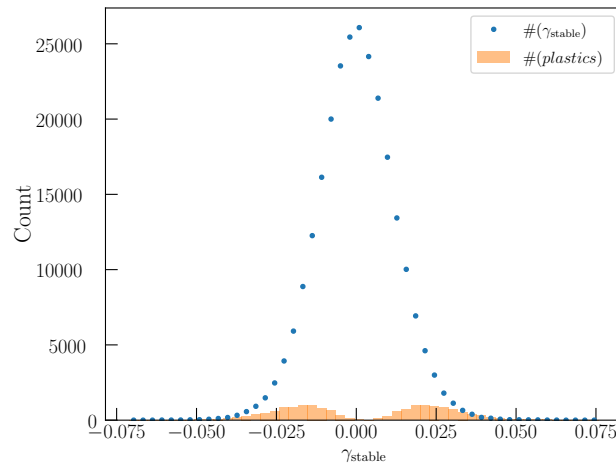


FIG. S3. Frequency distribution of strains required to attain shear-stability, in the *Zero-shear-stress* protocol, in systems of size  $N = 256$ . The orange bars indicate the number of plastic events encountered by samples that undergo strains in the corresponding intervals. They account for  $\sim 6.2\%$  of all samples. In the *Zero-shear-stress* protocol, we encounter plastic events during AQS. Here we show that the proportion of straining trajectories that encounter them, while small, is not insignificant.

### 4. Internal Bond-Stresses

#### a. Distributions

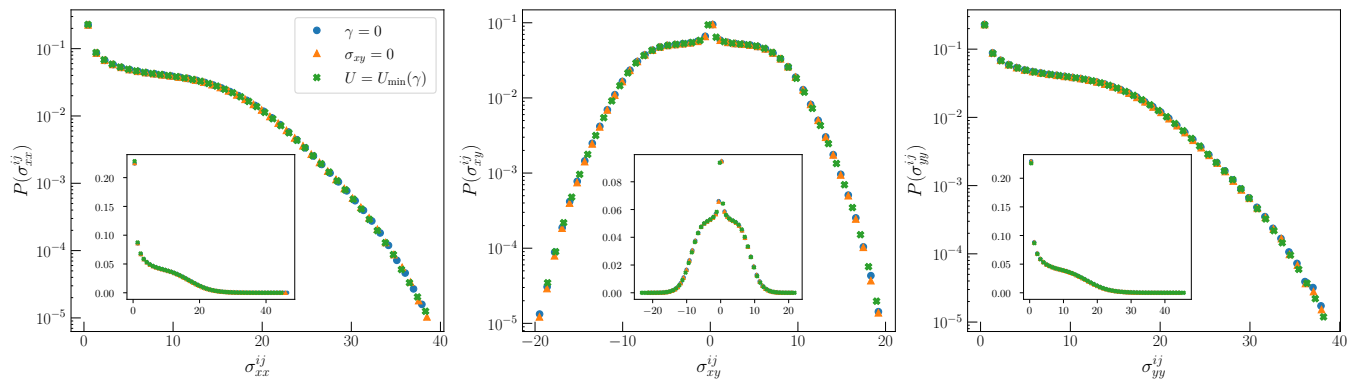


FIG. S4. Distributions of bond-stresses, from an ensemble of configurations of systems of size  $N = 256$ . The *Unstrained*, *Zero-shear-stress* and *Shear-strain-energy-minimized* ensembles all exhibit *identical* distributions.

#### b. Visualization



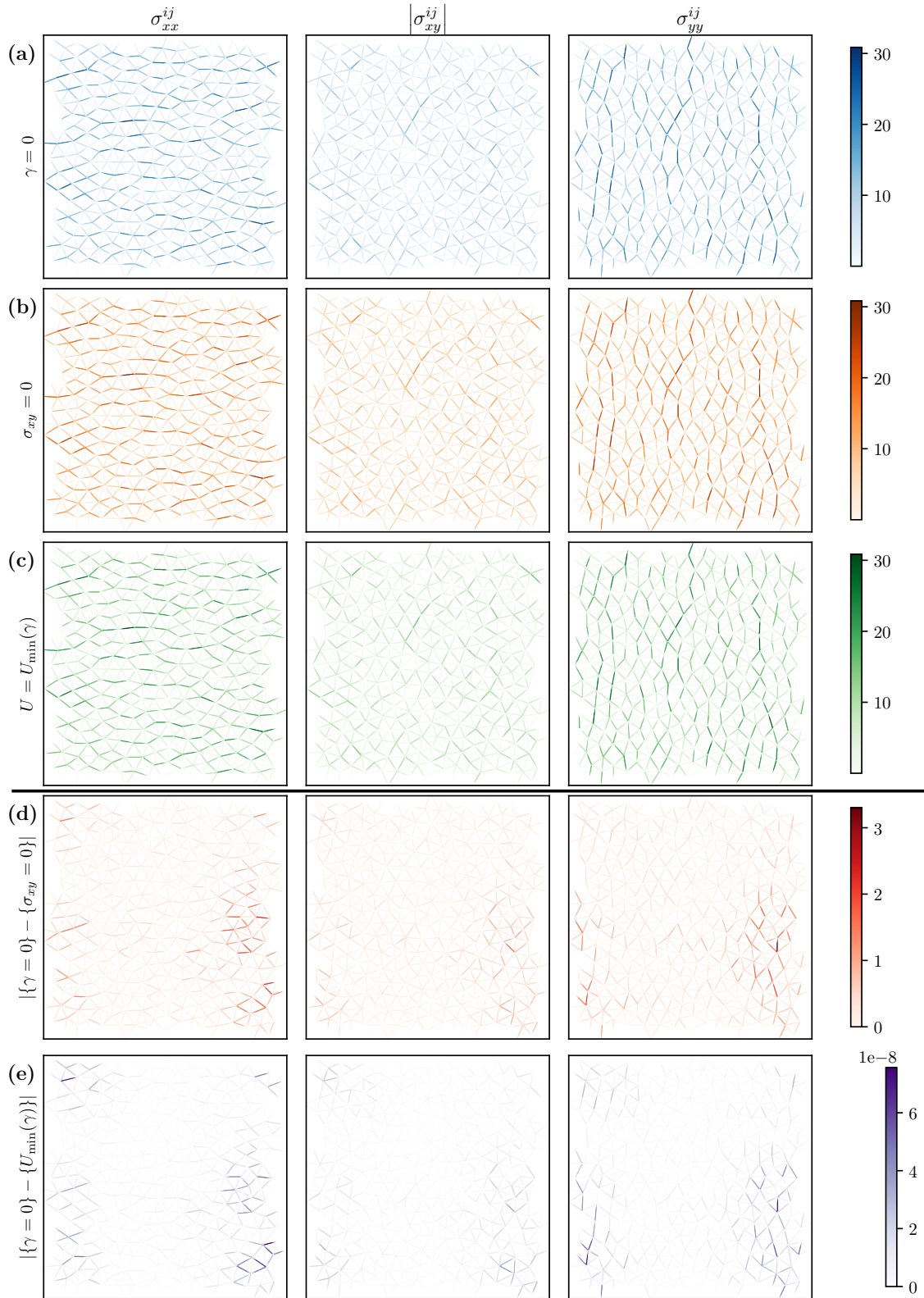


FIG. S5. Components of the stress tensor at each 'bond' in a two-dimensional configuration of a system of size  $N = 256$ . **(a)** an unstrained configuration, **(b)** The same configuration strained to achieve zero-shear-stress. **(c)** The same configuration as in **(a)**, energy minimized with a strain degree of freedom. **(d)** The difference in bond stresses between the *Unstrained* and *Zero-shear-stress* configurations is an order of magnitude smaller than the original stress. **(e)** The difference in bond stresses between the *Zero-shear-stress* and *Shear-strain-energy-minimized* configurations is zero up to numerical precision.

## 5. Large Systems

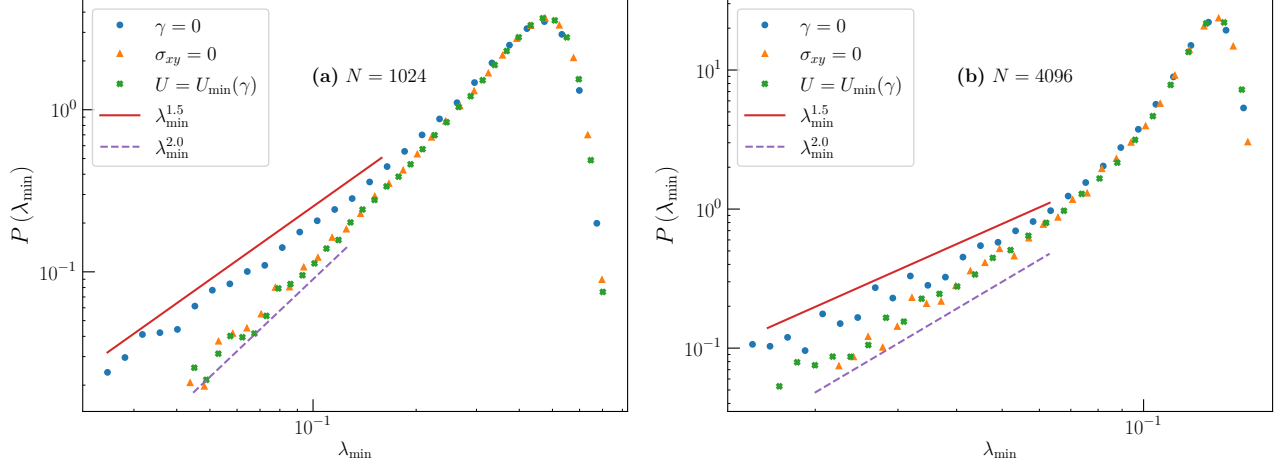


FIG. S6. Minimum eigenvalue distributions of the *Unstrained* and shear-stabilized ensembles in 2D, corresponding to larger system sizes: (a)  $N = 1024$  and (b) 4096. The lines indicate pure power-laws. The deviation from  $\omega_{\min}^4$  persists as larger system sizes are probed, and is not diminished with the suppressed stress fluctuations shown in Fig. S2.

## 6. Approach to Universal Distribution

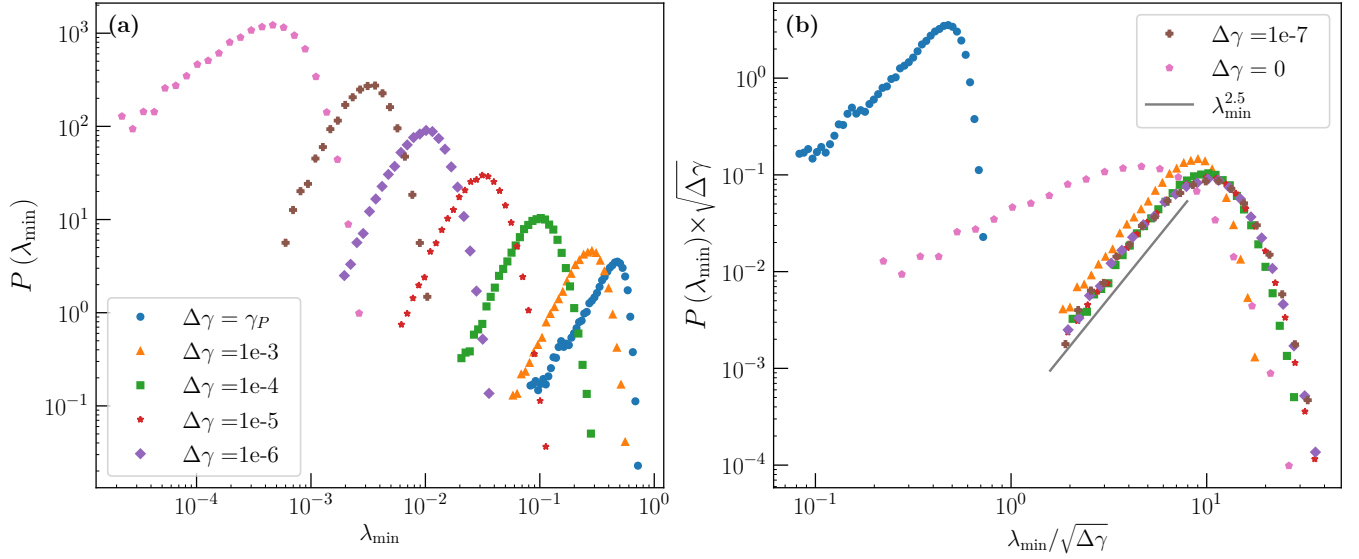


FIG. S7. Minimum eigenvalue distributions of a system of size  $N = 1024$ , upon approaching a plastic event. The (blue) circles display the distribution of eigenvalues in the initial, unstrained state. The (pink) hexagons are distributions of eigenvalues measured at closest approach to the plastic strain  $\gamma_P$ . The other distributions belong to ensembles of structures at specific strains away from  $\gamma_P$ .

## 7. Additional Simulation Details

### *Simulation Potentials*

We simulate a 50:50 mixture of two particle types A and B. The interaction potentials are cut-off at a distance

$$r_c = 1.385418025 \sigma, \quad (5)$$

with the three interaction diameters given by

$$\begin{aligned} \sigma_{AA} &= 1.0, \\ \sigma_{BB} &= 1.4, \\ \sigma_{AB} &= \sqrt{\sigma_{AA}\sigma_{BB}}. \end{aligned} \quad (6)$$

The only difference between the parameters in two and three dimensions of this model are the reduced number-densities given by

$$\begin{aligned} \rho_{2D} &= 0.85, \\ \rho_{3D} &= 0.81. \end{aligned} \quad (7)$$

In our simulations we focus on the purely repulsive pairwise potential, given by a tenth order polynomial, termed ‘R10’. The potential smooth to  $n$  derivatives at cut-off is given by

$$\psi = \left(\frac{\sigma}{r}\right)^{10} + \sum_{m=0}^n c_{2m} \left(\frac{r}{\sigma}\right)^{2m} \quad (8)$$

where the constants are calculated appropriately. We use only even-powered polynomials in order to avoid the potential curving downwards at the cutoff, to any precision, thus eliminating any attraction at the cutoff.

### *Sample size*

TABLE I. Number of minimum eigenvalue samples collected toward binning the  $P(\lambda_{\min})$  histograms plotted in Figs. 1 and S6. The suffix ‘K’ indicates a thousand.

Dimension	2			3
System size ( $N$ )	256	1,024	4,096	512
Samples	256K	256K	150K	256K

TABLE II. Number of minimum eigenvalue samples collected toward binning the *Plastic-event approach*  $P(\lambda_{\min,2,3})$  histograms plotted in Figs. 3, 4 and S7. The suffix ‘K’ indicates a thousand.

Dimension	2		
System size ( $N$ )	256	1,024	4,096
Samples	256K	50K	50K

### *Software*

Simulations of glasses along with the energy minimizations were performed using LAMMPS [59, 60]. The stopping criterion for the minimization was the force 2-norm:  $\sqrt{\sum_{i=1}^N |F_i|^2}$ . Eigenvalue calculations were performed using the LAPACK [61] routine: `dsyevr`, for small systems, and the Intel MKL [62] sparse solver routine: `mk1_sparse_d_ev`, for large-sized matrices. Analyses were performed with the help of NumPy [63–65] and SciPy [66, 67] libraries. Plotting was performed using Matplotlib [68, 69].

*Athermal Ensembles*

*Unstrained ensemble:* In our simulations, we use two-dimensional glass formers with varying particle numbers  $N \in \{256, 1024, 4096\}$  and a three-dimensional system of size  $N = 512$ , equilibrated at a parent temperature  $T_p = 0.58$ . We then cool to near-zero temperature at a slow rate of  $\dot{T} \approx 10^{-2}$ . We then employ the conjugate gradient algorithm to achieve an energy minimized state up to a force tolerance of  $1.0 \times 10^{-10}$ . These configurations constitute the *Unstrained* ensemble. We also use these configurations to generate the shear-stabilized ensembles.

*Zero-shear-stress ensemble:* We begin with a configuration drawn from the *Unstrained* ensemble and calculate the total shear stress ( $\sigma_{xy}$ ). We then strain the configuration in the direction of the stress. For example, if the shear stress is negative, then the system is strained towards the *left*. This choice of straining direction is determined by the direction of the initial stress in each configuration. This causes the stress to decrease in magnitude, and we proceed until the stress reverses direction. We perform the same operation two more times, each time with decreasing strain increments. The three strain steps we use are:  $\Delta\gamma \in \{5 \times 10^{-5}, 10^{-8}, 10^{-11}\}$ . The eigenvalues typically were not seen to vary much beyond the first strain step, but we proceed to ensure that we are not separated from the shear-stabilized state by a plastic event. When performing Athermal Quasi-static Shearing (AQS), we use Lees-Edwards boundary conditions, and strain at an engineering strain rate of  $5.0 \times 10^{-5}$ . At every step, the structure is relaxed to its minimum energy, to a force tolerance of  $1.0 \times 10^{-10}$ .

*Shear-strain-energy-minimized ensemble:* The configurations were generated using the LAMMPS procedure `box/relax`. The primary utility of this algorithm is that it allows one to perform energy minimizations allowing the shape of the simulation box to change, while also maintaining periodic boundaries. We make use of the procedure with only the shear-strain included as a degree of freedom aside from the particle positions. As highlighted in the documentation [60], this method encounters issues due to the algorithm utilizing the initial, un-strained box dimensions as a reference for the stress computation. The effect of this is that configurations that are at a large strain away from an stable state as well as those configurations that suffer plastic events before attaining shear-stability, both fail to achieve minimization to the desired force tolerance. This is remedied, as suggested in the documentation, in two ways: first by utilizing the `nreset` option to recalculate the reference box dimensions, and second by restarting the minimizer upon failure, typically across plastic events.

*Plastic-event-approach ensemble:* Plastic events are said to have occurred when there are non-affine displacements with a localized spatial extent and a small fraction of participating particles. These displacements differ from the typical elastic, affine response of the particles to the applied strain, most significantly in that the total magnitude of the displacement are much larger. An important feature of these events is the quadrupolar nature of the displacement field, centered at the point of localization, signaling a *T1*-like event. In order to ‘detect’ a plastic event, we utilize a convenience of the AQS protocol, being that every step of straining involves two stages: (a) application of an affine strain and (b) an energy minimization. Plastic events present large displacements in stage (b) of the protocol. Therefore, we keep track of the displacement of the maximally displaced particle at every step of energy minimization, and we register a plastic event when that value crosses a threshold. For our model, we use a value of  $\approx 15 \times \delta\gamma$ , whereas under elastic conditions, the maximum displacements during minimization are  $\sim \delta\gamma$ . Additionally in order to avoid some corner-case scenarios, we also utilize a minimum energy threshold of  $10^{-9}$  energy units for a step to register as a plastic event at a particular strain ( $\gamma_P$ ).

Given such a mechanism to detect plastic events, we now define an ensemble of configurations that all need the same ‘strain’ to incur a plastic event ( $\Delta\gamma = \gamma_P - \gamma$ ). Note that  $\Delta\gamma > 0$ . In order to sample small enough values of  $\Delta\gamma$ , we first measure the plastic-strain,  $\gamma_P$  to an accuracy of  $10^{-8}$  by ‘back-tracking’ to a previous state upon encountering a plastic-event, and subsequently straining the system at the requisite precision. Thus, we are able to sample configurations of the system at various values of the strain-to-plastic-event:  $\Delta\gamma \in \{10^{-3}, 10^{-4}, 10^{-5}, 10^{-6}, 10^{-7}\}$ .